Whiffletree based supports for self-adjustable hydrostatic bearings

van Parijs, Vincent; Nijssen, Joep; van Ostayen, Ron

Citation (APA)
van Parijs, V., Nijssen, J., & van Ostayen, R. (2021). Whiffletree based supports for self-adjustable hydrostatic bearings. *Advances in Mechanical Engineering*, *13*(12). https://doi.org/10.1177/16878140211055573

Important note
To cite this publication, please use the final published version (if applicable).
Please check the document version above.

Research Article

Whiffletree based supports for self-adjustable hydrostatic bearings

Vincent van Parijs, Joep Nijssen and Ron van Ostayen

Abstract

Hydrostatic bearings are superior in terms of their friction and load carrying characteristics when compared to contact based bearings, but non-usable in applications with non-constant curvature counter surfaces. A possible solution to this limitation is the introduction of deformable hydrostatic bearings components that cope with these required deformations. To reduce the required deformation of a single bearing pad, multiple pads can be connected through a so-called whiffletree support system. In this work, a symmetric whiffletree based hydrostatic bearing embodiment is introduced. A 2D quasi-static model is introduced that allows for determining the kinetostatic and path following properties of such a type of bearing. Design considerations are given regarding the joint rotational-, normal-, and shear stiffness of each individual joint, as well as basic bearing layout. The potential of a whiffletree suspended bearing is presented through the use of a case study.

Keywords

Whiffletree, hydrostatic bearing, deformable bearings, compliant mechanisms, mechanism design

Introduction

Hydrostatic bearings have the property of obtaining a high load capacity while maintaining low friction. This is due to the small fluid film between bearing and counter surface. Compared to conventional slider and roller bearings in terms of friction, wear, and load capacity, hydrostatic bearings are the better option. However, conventional hydrostatic bearings are limited to applications that have an external pressure source and constant or zero curvature counter surfaces.[1] To eliminate the second limitation, compliant hydrostatic bearings could provide a solution. Compliant hydrostatic bearings offer the ability to deform, following the counter surface while maintaining its desired constant film height. One approach to design compliant hydrostatic bearings, is to design the support to be elastic. This has been used to counter waviness of the counter surface,[2,3] to maintain load capacity when the bearing is tilted[4] or to function as an elastic pivot.[5] However, these type of supports are generally limited to small deformations in the order of the bearing film height.[2,6] This results in an absence of hydrostatic slider bearing use in applications with non-constant curvature counter surfaces. Examples of such potential applications can be found in motors and pumps, in civil structures like lock gates, and in sliding rooftops of stadiums.[3,7,8] A wide variety of potential applications could thus benefit from improved path-following functionality. This work will focus on the design of a large deforming hydrostatic bearing able to follow a non-constant curvature counter surface.

Delft University of Technology, Delft, The Netherlands

Corresponding author:
Ron van Ostayen, Delft University of Technology, Mekelweg 2, Delft 2600 AA, The Netherlands.
Email: R.A.J.vanOstayen@tudelft.nl

For hydrostatic bearings it is fundamental that the bearing and the counter surface remain close to parallel.[9] This means that, for a non-constant curvature counter surface, the bearing needs to deform to maintain a parallel orientation with respect to the counter surface. It is expected that the required deformation of the bearing, in order to maintain a parallel orientation to the counter surface, decreases as the length decreases. This is expected, as the curvature of the counter surface becomes close to linear if the length of the curvature decreases. However, a decrease in bearing length results in a decrease in load capacity which is undesirable for most applications. A solution could be to connect multiple smaller bearing pads, also called slipper, together by the use of a support structure.[10] This way, the deformation required from each slipper to maintain a close to parallel orientation with the counter surface, is reduced while load capacity could be maintained. A possible suitable support system is the whiffletree.[11] Examples of applications that use a whiffletree as support are dual-arm manipulators and telescopes.[11–14] It is important that conventional contact-based joints are not used in the support system of the hydrostatic bearing since they would re-introduce wear, friction, and backlash into the system. Hydrostatic spherical joints[15] or compliant joints[16,17] could solve these drawbacks, providing the same motion as conventional contact joints without these negative properties,[18] although in the case of compliant joints this generally comes at the cost of load capacity.[16] For the design of such a complete whiffletree based system, knowledge is needed about the kinematics and kinetostatics such that the potential quasi-static performance can be defined.

Previous research has shown that the use of elastic support systems allow hydrostatic bearings to follow surfaces with non-constant curvature.[2–6] In this previous work it was concluded that elastic supports do improve the deformability of hydrostatic bearings but only for deformations with an order of magnitude of the nominal film height. The contribution of this work is to design a support system that allows deformations orders of magnitude larger than the nominal film height.

In this paper, a symmetric whiffletree based suspension for deformable hydrostatic bearings is introduced. A 2D quasi-static model based on rigid body mechanics is presented that can be used to define the general kinematics, more specifically the rotational requirements for individual joints. Design steps are provided to determine load capacity, normal stiffness, rotational stiffness, shear stiffness, and pressure profiles of such symmetric whiffletree based bearing systems. The model is then implemented in a case study to show the potential of these type of supports.
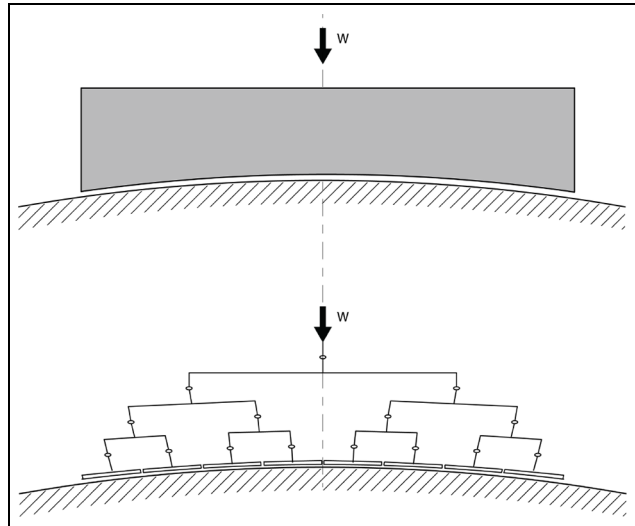
Figure 1. Elasto-hydrostatic bearing in its deformed configuration to remain parallel with the counter surface (top) and a whiffletree supported hydrostatic bearing in its deformed configuration to remain parallel with the counter surface (bottom).

Methods

The 2D whiffletree based large deforming hydrostatic bearing is presented in this work as an alternative to compliant support bearings as shown in Figure 1. In literature,[1] large deformable bearings are defined as bearings that (a) are able to deform $\geq 10\%$ of the height of the bearing in its undeformed configuration, and (b) are able to deform ≥ 100 times the average film height of the fluid film. The implementation of compliance to obtain large deformation in full film bearings is a significantly more difficult challenge compared to their small deforming counterparts, simply because large compliance and high load capacity are not necessarily aligned design objectives. If an elastic support, called slipper in this work, is utilized for these objectives, then all required motion has to come out of a single geometry. This geometry is not necessarily designed for motion, but to obtain a certain load capacity. A whiffletree based bearing support gives a different perspective to the same design challenge. By introducing discrete components specifically designed for the load case, the load can potentially be better distributed while maintaining deformability. The whiffletree support is used to reduce the required slipper deformation by allowing each slipper to rotate, obtaining a better orientation to the counter surface. This advantage is one of the principle motivations for introducing the whiffletree support system and thus will first be analyzed in detail. Because primary motivation in this work is to introduce the whiffletree suspension as a
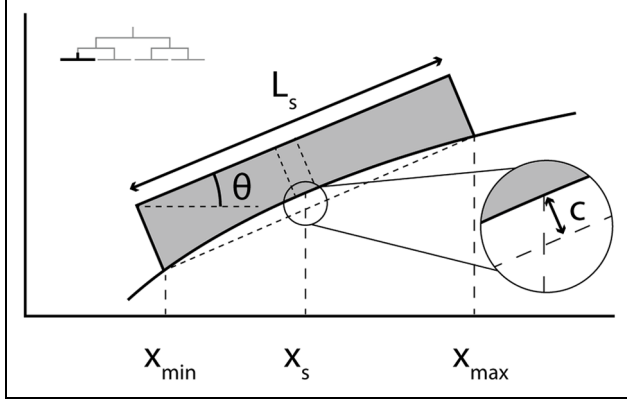
Figure 2. Single slipper compressed to remain parallel to the track with the corresponding parameters.

Figure 3. Compression required of a single slipper, as function of the slipper length for a counter track with an amplitude of 5%, 10%, and 15% of the wavelength respectively.

design alternative, all modeling performed in this work will be done in 2D. In accordance with what has been observed in literature,[3,19,20] the counter surface or track of the system will be represented by a sine wave with wavelength λ and amplitude A. Bearing deformation, as function of its length, can be expressed as the slipper compression required to maintain a parallel orientation with the track as seen in Figure 1. Figure 2 shows a slipper in its deformed configuration while maintaining a parallel position with the gradient of the counter surface. The minimum and maximum positions of the track under the slipper, which is a specific track section in the slippers reference frame, are required for determining slipper compression. The specific track section is obtained by finding the x position of both edges of the slipper $x_{\mathrm{min/max}}$ described as:

$$x_{\mathrm{min/max}} = x_{\mathrm{s}} \pm \frac{1}{2} L_{\mathrm{s}} \cos(\theta) \tag{1}$$

where x_{s} is the x position of the slipper center, L_{s} is the slipper length, and θ the angle of slipper center point with respect to the horizontal. The specific track section U is now defined by:
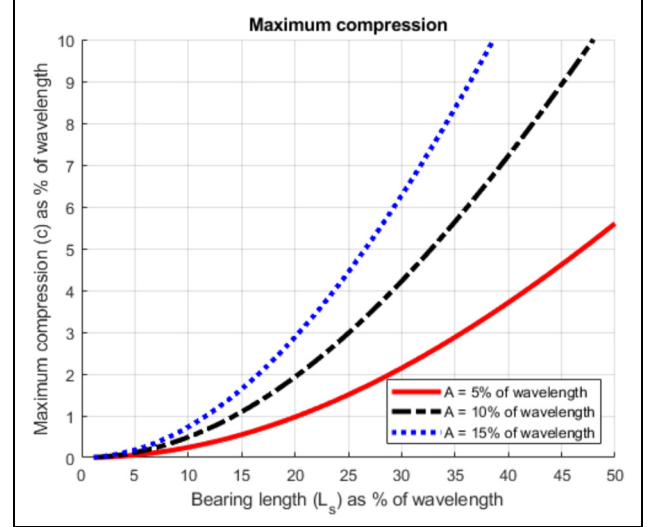
$$U = \begin{bmatrix} x \\ y \end{bmatrix} = \begin{bmatrix} x \\ A\sin\left(\frac{2\pi x}{\lambda}\right) \end{bmatrix} \text{ for } x_{\mathrm{min}} \leqslant x \leqslant x_{\mathrm{max}} \tag{2}$$

where A is the amplitude of the track and λ is the wavelength of the track. The specific track section is placed at the origin defined by:

$$U_{\mathrm{translated}} = U - T \tag{3}$$

where T is the translation matrix defined by:

$$T = \begin{bmatrix} x_{\mathrm{s}} \\ A\sin\left(\frac{2\pi x_{\mathrm{s}}}{\lambda}\right) \end{bmatrix} \tag{4}$$

Next, the specific track section is rotated such that the gradient of the track at position x_{s} is orientated parallel to the horizontal defined by:

$$U_{\mathrm{final}} = R \cdot U_{\mathrm{translated}} = \begin{bmatrix} x' \\ y' \end{bmatrix} \tag{5}$$

where R is the rotation matrix described by:

$$R = \begin{bmatrix} cos(\theta_{\mathrm{s}}) & sin(\theta_{\mathrm{s}}) \\ -sin(\theta_{\mathrm{s}}) & cos(\theta_{\mathrm{s}}) \end{bmatrix} \tag{6}$$

where θ_{s} is described by:

$$\theta_{\mathrm{s}} = \arctan\left(\frac{y_{\mathrm{s}}}{x_{\mathrm{s}}}\right) \tag{7}$$

Finally, the linear compression c of the slipper to remain parallel with its track is described by:

$$c = y'_{\mathrm{max}} - y'_{\mathrm{min}} \tag{8}$$

where y'_{min} and y'_{max} are respectively the minimum and maximum y values of the rotated specific track section. The slippers maximum required compression over the whole track is obtained by following the previous steps for each x_{s} position on the track. Figure 3 shows the maximum compression required as a function of the slipper length for a track amplitude of 5%, 10%, and 15% of the wavelength respectively. It can be seen that the relation between the compression and slipper length is approximately quadratic. This means that a decrease in slipper length of factor s will result in a decrease in compression of factor s^2. This beneficial effect can be captured through the implementation of a whiffletree
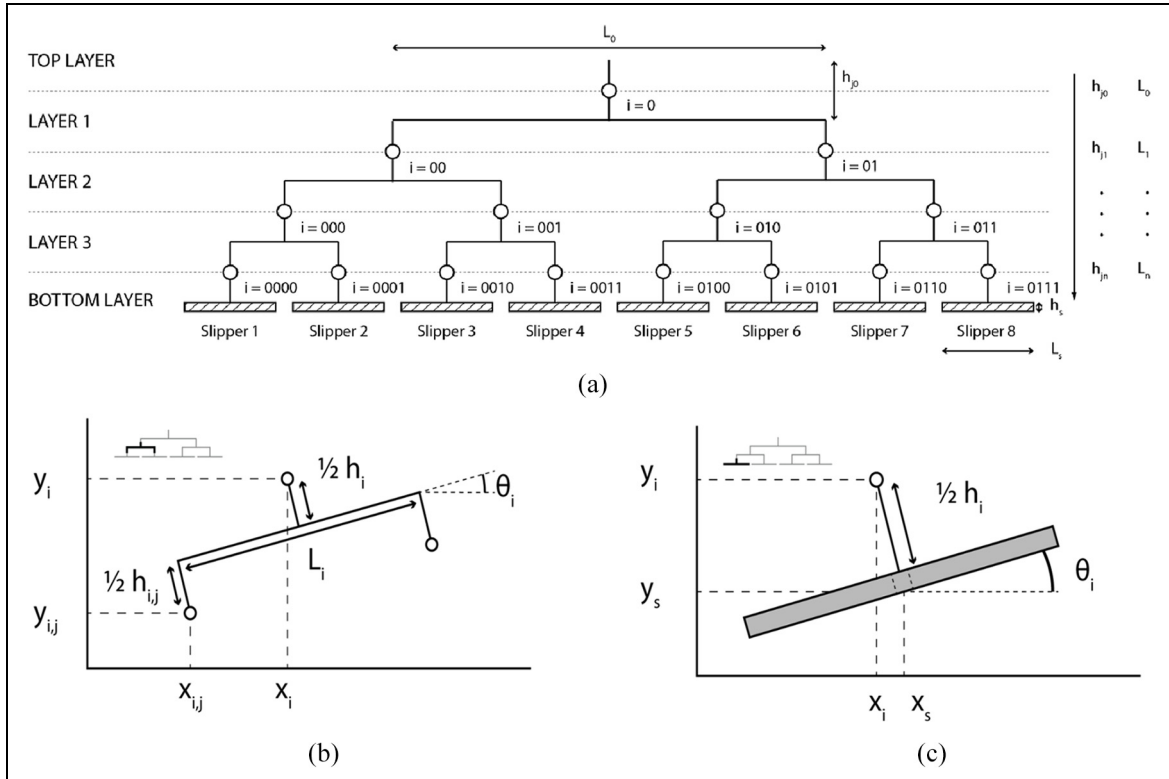
Figure 4. (a) Layout of a triple layer whiffletree support system with the corresponding layer, joint numbers, and total bearing height. (b) Whiffletree layer cell configuration consisting of three joints connected by a rigid linkage. (c) Bottom layer cell configuration consisting of a slipper connected to a single joint by a rigid linkage.

in the bearing suspension and functions as one of the primary motivations for developing such a support.

Bearing topology

Different embodiments can potentially be envisioned for these kind of support systems. The advantages for implementing these suspensions in hydrostatic bearings is that they allow for the implementation of discrete rotational components, specifically designed for the load case, while simultaneously distributing the load over the support. This, combined with the type of sinusoidal counter tracks investigated in this work, directly impact the topology. The following statements are made concerning the suspension topology investigated in this work:

1. The suspension will be used to follow symmetric variable counter surfaces.
2. The suspension will be used to fully distribute the load uniformly.

The first statement directly relates to the definition of using a sinusoidal wave as the basis for counter surfaces, and thus the expected type of deformations.

Using both statements, this work introduces the symmetric whiffletree suspension that can be seen in Figure 4 that will be the basis for the whiffletree support performance presented. For this topology, the height of the joint on the slipper is equal to half the slipper length and that the height of each joint in a layer is twice the length of the joint one layer below. The assumption in thus topology is that there is no distance between the slippers, which would not work in a practical embodiment. Since the focus of this work however is on the support and we minimize the impact of the slippers themselves, it is an accepted error. It is also avoidable in future practical embodiments by ensuring the slipper is smaller then L_s. This topology can be seen as the neutral design state for sinusoidal counter tracks, where the loads are equally distributed over the joints. Because of this symmetric positioning of the lower layers and all slippers design spaces being equal in size, it does not have any inherent changes in load between the individual joints in one layer. This means all joints in the same layer will experience the same load condition, be it with a phase difference. This topology therefore has equal load distribution based on its undeformed configuration. It therefore embodies the second statement and fully distributes the load uniformly.

The next important design dimension is the bearing height. Bearing height is built up out of the slipper height and the total joint height in the system as shown in Figure 4. The length of each joint L_k is defined by:

$$L_k = 2^{(n-k)}L_s \qquad (9)$$

where L_s is the slipper length and k is the layer in which the joint is located counted from top to bottom, n being the total number of whiffletree layers, and k being $n + 1$ for the layer containing the slippers. The height of a single joint, depending on its location in the whiffletree, is defined as:

$$h_j = uL_k \qquad (10)$$

where u is the joint height-to-length ratio. The total bearing height is defined by the sum of all joints as well as the total slipper height, which is dependent on the maximum allowed compression, defined as:

$$h_b = \frac{1}{e}c_{max} + \sum_{k=0}^{n} uL_k \qquad (11)$$

where n is the number of layers in the whiffletree, u the joint height-to-length ratio, c_{max} the maximum required compression, and e the maximum allowable compression of the slippers material. Beside the general dimension of the whiffletree, both its kinematics and kinetostatics will also be defined.

Bearing kinematics

A whiffletree based support fundamentally consists of multiple layers. Here, each layer contains a number of cells equal to the layer number, as shown in Figure 4.

In the proposed topology, each cell except for the bottom layer, has three joints connected by a rigid link as shown in Figure 4(b). The cells of the lowest layer consist of a slipper connected with a rigid link to a joint which is shown in Figure 4(c). The indexation used for the introduced topology is shown in Figure 4. As shown, parts in the top layer of the cell are noted with an i, and parts in the bottom layer of the cell are noted with $(i, 0)$ for the left part and $(i, 1)$ for the right part or (i, j) if both parts are defined.

To allow for an analytical definition of suspension kinematics, a rigid body based model will be introduced. The whiffletree kinematics are described by the linkage dimensions, the joint angles with respect to the horizontal and the joints x and y positions. All angles with respect to the horizontal are described by θ and all pivot angles of the joints are described by ϕ as shown in Figure 5.

The x and y position of each joint $x_{i,j}$ and $y_{i,j}$, as shown in Figure 4(b), are defined by:
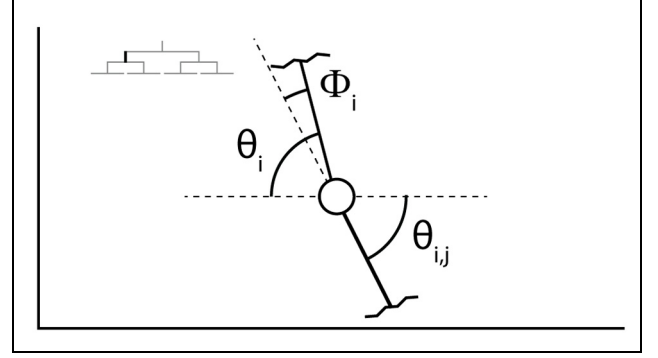
Figure 5. The angle of each linkage with the horizontal θ and the angle with respect to the linkage one layer above ϕ.

$$x_{i,j} = x_i \pm \frac{1}{2}L_i \cos(\theta_i) + \frac{1}{2}(h_i + h_{i,j})\sin(\theta_i) \qquad (12)$$

$$y_{i,j} = y_i \pm \frac{1}{2}L_i \sin(\theta_i) - \frac{1}{2}(h_i + h_{i,j})\cos(\theta_i) \qquad (13)$$

where L_i is the length of the linkage, h_i and $h_{i,j}$ are the joint heights, θ_i is the joint angle, and x_i and y_i are the respective joint x and y position, one layer above. As seen in equations (12) and (13), the position of each joint in a layer is described by the joints position in the ascending layer. The x and y position of the joint connected to a slipper x_i and y_i, as shown in Figure 4(c), are defined by:

$$x_i = x_s - \frac{1}{2}(h_i + h_s)\sin(\theta_i) \qquad (14)$$

$$y_i = y_s + \frac{1}{2}(h_i + h_s)\cos(\theta_i) \qquad (15)$$

where x_s and y_s are respectively the x and y position of the center of the slipper, h_i is the joint height, h_s is the slipper height, and θ_i is the joint angle. This gives the x and y position of the slipper as function of the slipper angle with respect to the horizontal. Assuming that the slipper remains parallel with the gradient of the track at position x_s, the angle θ_i is defined by:

$$\theta_i = \arctan(2\pi A \cos(2\pi x_s)) \qquad (16)$$

where A is the amplitude of the track. Furthermore, the y position of the center of the slipper is described by:
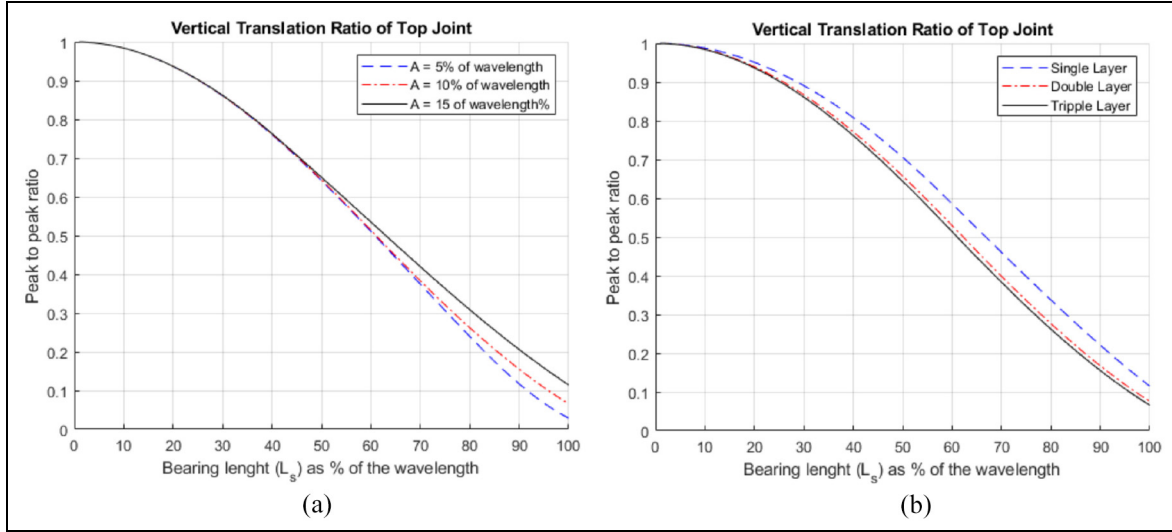
$$y_s = A \sin(2\pi x_s) \qquad (17)$$

When setting equations (16) and (17) equal to zero, so that they can be solved, the following set of equations is obtained:

$$\arctan(2\pi A \cos(2\pi x_s)) - \theta_m = 0 \qquad (18)$$

$$A \sin(2\pi x_s) - y_s = 0 \qquad (19)$$

Figure 6. (a) Peak to peak ratio of a triple layer whiffletree with a counter surface amplitude *A* of 5%, 10%, and 15% of the wavelength. (b) Peak to peak ratio for a single, double and triple layer whiffletree with a counter surface amplitude of 10% of the wavelength.

If the joint in the top layer is assumed to have a prescribed *x* position and a variable *y* position, the set of equations consisting of equations (18) and (19) can be obtained for each slipper. If the assumption holds that the slippers remain parallel with the gradient of the track, the system is fully constrained following Gruebler's equation resulting in a solvable system of equations.[21] If the system of equations is solved, the pivot angle ϕ of each individual joint is then defined by:

$$\phi_{i,j} = \theta_{i,j} - \theta_i \tag{20}$$

where $\theta_{i,j}$ is the corresponding joint angle with respect to the vertical and θ_i is the joint angle with respect to the vertical one layer above. Furthermore, the top joint *y* position can be obtained. So as described, the kinematics can now be obtained using the previously given equations. Using the top joint *y* position, the ratio between the peak to peak value of the top joint and the counter surface shown in Figure 6(a) and (b) can be obtained. The effect of different amplitudes compared to the wavelength and the effect of increased layer numbers is presented in these figures.

Bearing kinetostatics

Kinetostatic performance of the support is directly related to the stiffness of each individual joint. The directions of the rotational-, normal-, and shear stiffness of each joint are shown in Figure 7. In this work, the linearized rotational stiffness relative to the neutral configuration of the joint k_r being defined as:
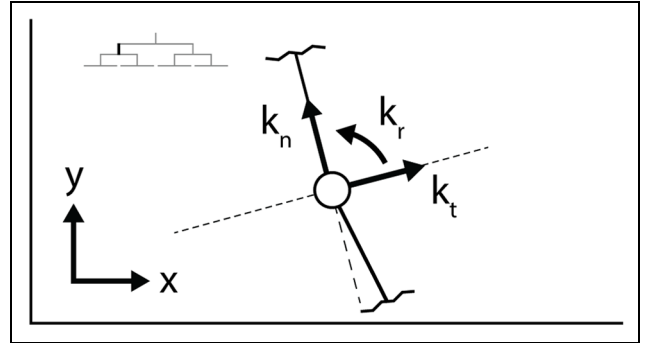
Figure 7. Normal-, shear-, and rotational stiffness acting on each individual joint in the whiffletree.

$$k_r = \frac{M_r}{\phi_r} \tag{21}$$

where M_r is the moment acting on the joint and ϕ_r is the pivot angle of the joint. The linearized normal stiffness relative to the neutral configuration of the joint k_n is defined as:

$$k_n = \frac{F_n}{\delta_n} \tag{22}$$

where F_n is the normal component of the force acting on the joint and δ_n is the allowable normal displacement of the joint. Finally, the linearized shear stiffness relative to the neutral configuration of the joint k_t is defined as:

$$k_t = \frac{F_t}{\delta_t} \tag{23}$$

where F_t is the tangential component of the force acting on the joint and δ_t is the allowable tangential displacement of the joint. As shown, these different types of stiffness are dependent on the moments and forces acting on each joint. The forces acting on each slipper are decomposed to correspond to the fixed x and y frame connected to the upper section of the whiffletree. The forces in x and y direction acting on each slipper F_x and F_y are defined by:

$$F_x = - W_s \sin (\theta_s) \tag{24}$$

$$F_y = W_s \cos (\theta_s) \tag{25}$$

where W_s is the load capacity of the slipper and θ_s is the angle of the slipper with respect to the horizontal. The load carrying capacity of a single slipper, for an equally distributed whiffletree support system where the load carrying capacity of the joints in each ascending layer doubles, is described by:

$$W_s = \frac{W_{\text{tot}}}{n} \tag{26}$$

where W_{tot} is the load carrying capacity of the system and n is the total number of slippers in the system. The forces acting on each joint $F_{x(i)}$ and $F_{y(i)}$ are then defined by:

$$F_{x(i)} = F_{x(i,0)} + F_{x(i,1)} \tag{27}$$

$$F_{y(i)} = F_{y(i,0)} + F_{y(i,1)} \tag{28}$$

To obtain the normal- and shear force acting on each joint, a second decomposition is used. The normal force F_n acting on each joint is defined by:

$$F_n = F_y \cos (\theta) - F_x \sin (\theta) \tag{29}$$

where θ is the angle of the joint with respect to the horizontal. The shear force F_t acting on each joint is defined by:

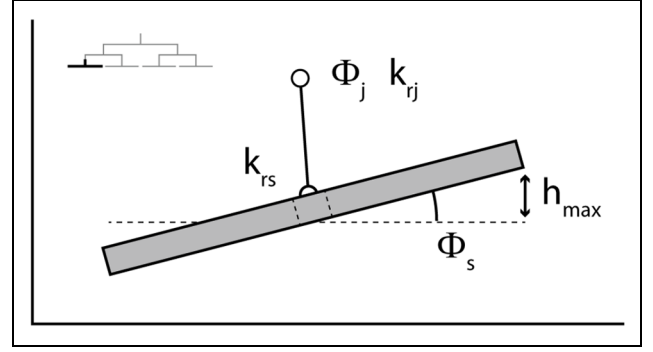$$F_t = F_y \sin (\theta) + F_x \cos (\theta) \tag{30}$$

The moment M_i acting on each joint, except for the joints connected to a slipper, is defined by:

$$M_i = F_{a(i)} \frac{L_i}{2} + F_{b(i)} \frac{(h_i + h_{i,j})}{2} + M_{i,0} + M_{i,1} \tag{31}$$

where h_i and $h_{i,j}$ are the joint heights and L_i is the linkage length as shown in Figure 4(b) and $F_{a(i)}$ and $F_{b(i)}$ are defined by:

$$F_{a(i)} = F_{y(i,0)} \cos (\theta_i) - F_{x(i,1)} \sin (\theta_i) \tag{32}$$

$$F_{b(i)} = F_{y(i,0)} \sin (\theta_i) - F_{x(i,1)} \cos (\theta_i) \tag{33}$$

Figure 8. Representation of a slipper with a hinge joint connecting the slipper and bottom layer joint together and the corresponding parameters.

where θ_i is the angle of the joint with the horizontal. The moment acting on the joints connected to the slipper is defined by:

$$M = \int xPdx \tag{34}$$

where P is the distributed load acting on the slipper. The rotational stiffness of each individual joint can now be obtained. Furthermore, the normal- and shear stiffness of each individual joint is given as a function of the maximum allowable displacement in the normal and tangential direction.

With the rotational stiffness of each individual joint known, the relation between the tilt stiffness of each slipper and their corresponding bottom layer joint is found. The linearized tilt stiffness relative to the neutral configuration of the slipper k_{rs} is defined by:

$$k_{rs} = \frac{M_s}{\phi_s} \tag{35}$$

where M_s is the moment acting on the slipper and ϕ_s is the slipper angle with respect to the gradient of the track at position x_s. The tilt stiffness of the slipper is modeled as a hinge joint between the slipper and the bottom layer joint as seen in Figure 8. The maximum tilt stiffness of the slipper is related to the maximum pivot angle of the slipper ϕ_{smax} which is defined by:

$$\phi_{smax} = \arcsin \left(\frac{2h_{\max}}{L_s} \right) \tag{36}$$

where $h_{\max}$ is the maximum allowable deviation in the film height and L_s is the slipper length. The maximum allowable angle of the slipper prevents solid to solid contact between the slipper and track due to tilting of the slipper. However, it is desired that the influence of the tilt stiffness of the slipper on the system is negligibly small. Meaning the hinge joint between the slipper and bottom layer joint in Figure 8 can be seen as a rigid

connection. To assure this, a high tilt stiffness of the slipper is required with respect to the rotational stiffness of the bottom layer joint. This relation is dependent on the angle of the slipper and the angle of the bottom layer joint which is defined by:

$$k_{rs} = \frac{k_{rj}\phi_j}{\phi_s} \qquad (37)$$

where ϕ_j is the bottom layer joint pivot angle and k_{rj} is the bottom layer joint rotational stiffness. With the given equations, the kinetostatics of the whiffletree can now be obtained. To position the whiffletree in every configuration that is required to follow the track, at every step a difference in load capacity on each slipper is required. The difference in load capacity on the slippers generates a moment acting on each joint, resulting in a rotation of the joint. This difference in load capacity is obtained by changing the film height under each slipper. The relation between the load capacity and film height can be found in the 1D Reynolds equation,[9] showing that a decrease in film height results in an increase in load capacity. Since the focus of this work is on the support, the modeling of the slipper load capacity is not further discussed as it falls outside of the scope. The total change in film height of each slipper is dependent on the joints that are related to the slipper and the rotational direction of these joints. For a joint to rotate counter clockwise (ccw), the corresponding slippers right of the joint should have a higher load capacity compared to the corresponding slippers left of the joint. For a joint to rotate clockwise (cw), the corresponding slippers left of the joint should in combination exert a higher force moment compared to the corresponding slippers right of the joint. As an example, looking at Figure 4, for joint 11 to make a ccw rotation, slipper 3 and 4 need a decrease in film height while slipper 1 and 2 remain an equal or have an increase in film height. It is important that the total change in film height should not exceed the minimum film height under each slipper in the undeformed configuration, since this would re-introduce solid-solid contact.

Design rules

The sections before presented the general model for the symmetric whiffletree bearing consisting out of the following components: bearing design dimension, kinematics, and kinetostatics. Based on this model, the following rules of thumb can be introduced to aid designers in their design process, given the large degree of design freedom this whiffletree based support offers. Based on the previous models, the following rules should be followed:
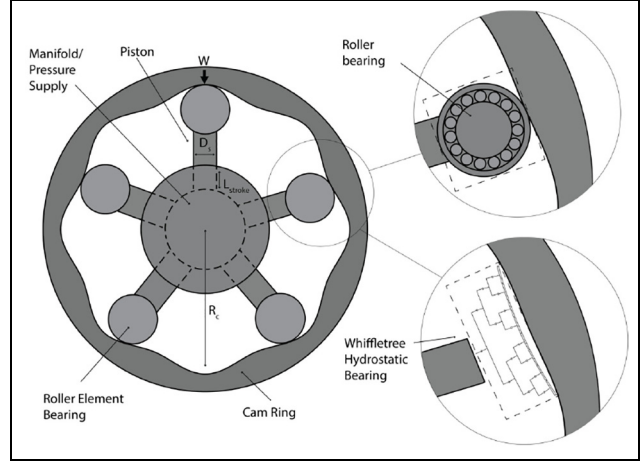
Figure 9. Schematic overview of the radial pump used in the case study where the conventional roller bearing and the newly obtained whiffletree supported hydrostatic bearing are shown.

1. Minimize the slipper length given the maximum slipper compression, number of whiffletree layers, and bearing length for the smallest bearing design dimension.
2. Increase the number of whiffletree layers given an increase in bearing length for smallest bearing design dimension.
3. Minimize the joint rotational stiffness.
4. Maximize the joint normal- and shear stiffness.
5. Maximize the ratio between slipper tilt stiffness and bottom layer joint rotational stiffness.

For validation, the models and design rules will be implemented in a case study.

Design case study

To validate the model and show the potential of this type of support a case study is used. A potential application that currently is not able to make use of the performance characteristics of hydrostatic bearings, is the radial piston pump. Especially the variant where cam rings are implemented,[7] which have counter surfaces with a sinusoidal shape, use roller bearings exclusively because of this constantly varying track. An example of such a pump topology can be seen in Figure 9.

A case study is presented based on the general dimension and performance criteria of an experimental water pump used in the power train of a water hydraulic wind turbine.[7,22] The objective of this case study is to show the effect of design choices for the whiffletree support, while simultaneously providing the reader with the required kinematic and kinetostatic criteria that should be strived for when implementing this

Table 1. Parametric values used in the case study.

Description	Parameter	Value	Unit
Piston diameter	D_s	0.06	m
Cam ring wavelength	λ	0.45	m
Piston stroke	L_{stroke}	0.03	m
Cam ring radius	R_c	0.5	m
Cam ring amplitude	A	0.023	m
Supply pressure	P_s	80E5	Pa
Bearing load	W	17	kN
Joint height to length ratio	u	1	–
Max compression slipper	c_{max}	0.1	–
Allow. normal displacement joints	δ_n	$0.01h_j$	m
Allow. tangential displacement joints	δ_t	$0.01h_j$	m
Total bearing length	L_{tot}	0.5λ	m

support in comparable applications. The operating conditions as well as geometrical constraints are defined in Table 1. The main components are the cam ring, piston, and pressure supply source that define this design case. As seen in Figure 9, the bearing is connected to a piston and follows the path described by the cam ring surface. The fluid pressure in the piston is also used as the bearing pressure supply. To simplify this case study, the output pressure is assumed to be equal for the entire stroke cycle. This represents the highest load case. Since this is a case study that solely investigates the kinematics and kinetostatics of the potential support, an example joint is implemented of which the joint to height ratio, the allowable normal

displacement, and the tangential displacement are defined. For the slipper solely the maximum compression criteria is defined. These characteristics are dependent on the joint used and primarily depend on its failure criteria, which fall outside the scope of this work. This example will compare a single, double, and triple layer whiffletree support. The visualization of the three embodiments are presented in scale in Figure 10. To obtain the desired piston stroke L_{stroke} that needs to be followed, in accordance to Figure 6(a), the total bearing length is chosen to be 0.5λ. The maximum allowable film height deviation allowed in this case study equals 40%.

The final parameter that effects the dimension of the whiffletree support is the bearing to wavelength ratio. The effect of this parameter is visualized in Figure 11. A sole slipper with rotational hinge is added as reference.

The way this model is set up is such that it can be used by designers to determine the maximum total bearing dimension, required joint rotations, shear and normal stiffness given this set of input parameters.

Model validation

To validate the model, a comparison is made between the analytical model and a Finite Element Model (FEM) using Comsol Multiphysics and the multibody dynamics module. The linkages are modeled as rigid beams, using the rigid domain function and the joints are modeled as hinge joints. The top joint has a prescribed x position, a variable y position and is constrained in rotation. The slippers have a prescribed y_s
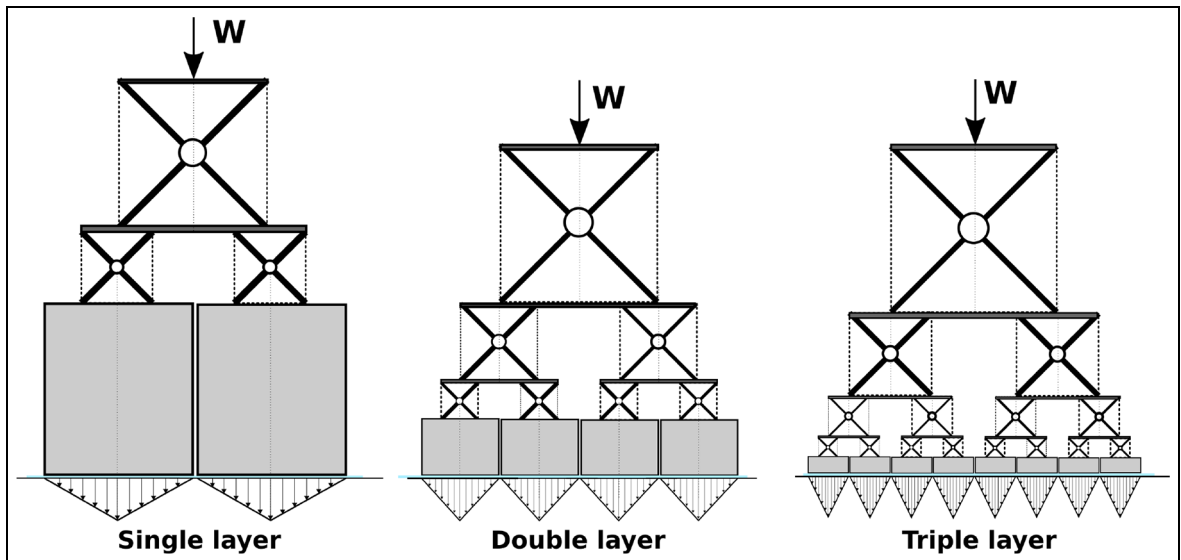
Figure 10. To scale dimensionless comparison between the three proposed whiffletree embodiments. The increased number of layers has a positive influence on the total bearing height, given equal bearing length.
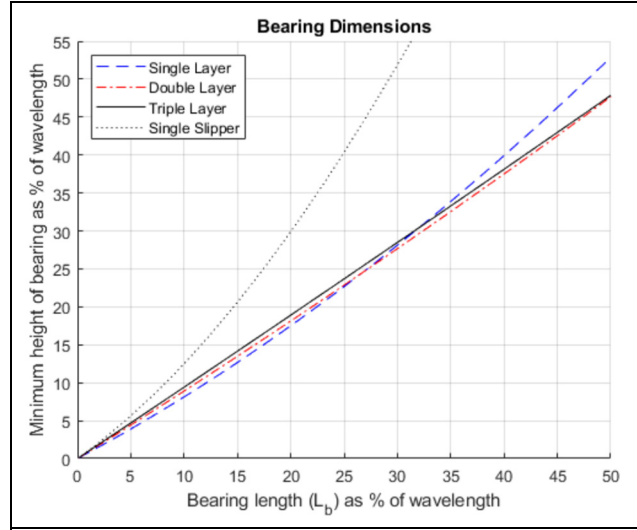
Table 2. Minimum rotational stiffness and maximum normal and shear force acting on each individual joint in their corresponding layer.

Type	Description	Parameter	Value	Unit
Single layer	Joint height (top)	h_t	0.113	m
	Joint height (1)	h_1	0.056	m
	Slipper length	L_s	0.113	m
	Slipper height	H_s	0.154	m
	Total dimension	$L_{tot}H_{tot}$	0.073	m²
Double layer	Joint height (top)	h_t	0.113	m
	Joint height (1)	h_1	0.056	m
	Joint height (2)	h_2	0.028	m
	Slipper length	L_s	0.056	m
	Slipper height	H_s	0.039	m
	Total dimension	$L_{tot}H_{tot}$	0.0531	m²
Triple layer	Joint height (top)	h_t	0.113	m
	Joint height (1)	h_1	0.056	m
	Joint height (2)	h_2	0.028	m
	Joint height (3)	h_3	0.014	m
	Slipper length	L_s	0.028	m
	Slipper height	H_s	0.01	m
	Total dimension	$L_{tot}H_{tot}$	0.497	m²

Figure 11. Percentage wise effect of increasing the number of whiffletree layers as function of the bearing length/wavelength has on the total bearing height.

position and angle θ as function of its x_s position, which are given by equations (16) and (17). In the simulation, the top joint travels for a full wavelength. The validation will solely be performed on the triple layer whiffletree configuration, since this is the highest geometrical order model analyzed in this case study.
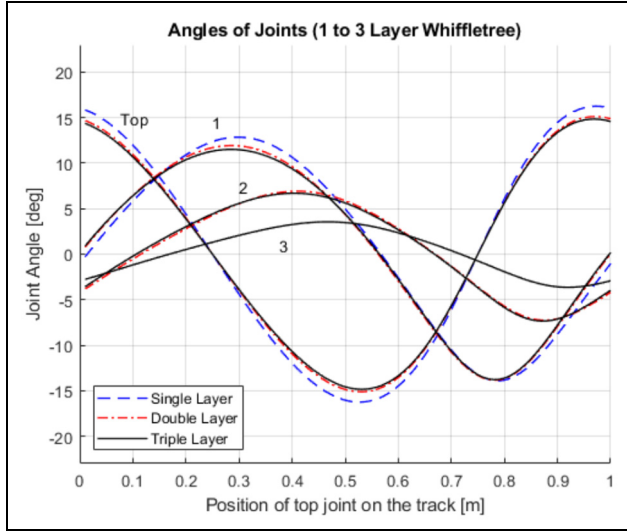
Results

Following the presented method of determining the bearing topology, the design dimension for all three

embodiments of the symmetric whiffletree support can be seen in Table 2. Please note that any rigid connection members do not have a dimension in this work and therefore do not effect the total design dimension.

Based on these dimensions, both kinematic and kinetostatic performance of all three embodiments are presented in Figure 12(a) and (b). Figure 12(a) shows the comparison of the FEM model with the analytical version presented in this work for a triple layer symmetric whiffletree. Only the leftmost joint angle of each layer is shown since the remaining joints in the same layer show equal behavior with the difference of a phase shift. The
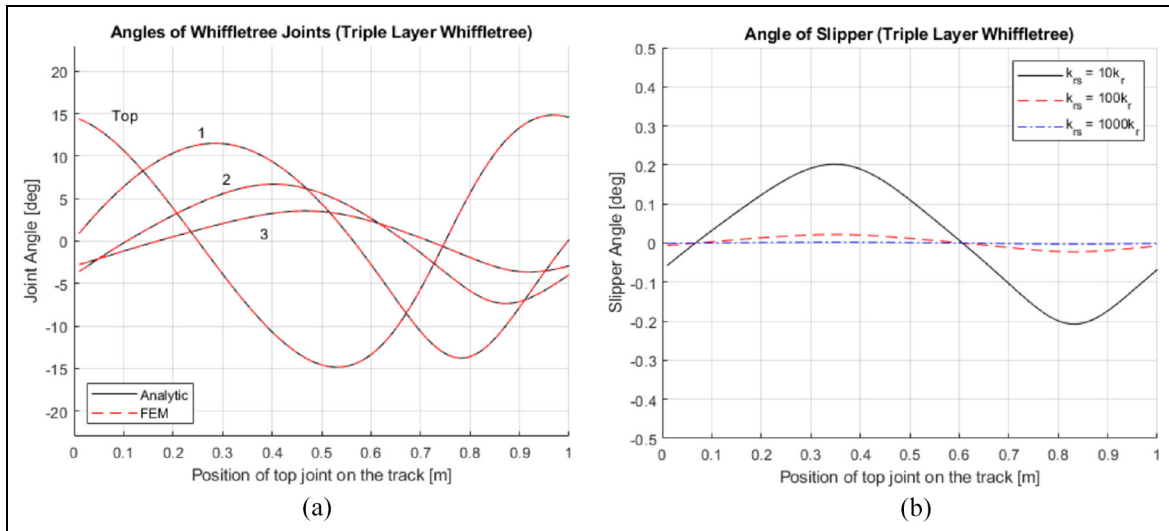
Figure 12. (a) Joint pivot angles of the FEM and analytical model compared for a triple layer whiffletree. (b) Slipper pivot angle of a triple layer whiffletree with a rotational stiffness ratio of 10, 100, and 1000.

Figure 13. Joint pivot angles of a single, double, and triple layer whiffletree compared.

Table 3. Minimum rotational stiffness and maximum normal and shear force acting on each individual joint in their corresponding layer.

Description	Parameter	Layer	Double	Triple	Unit
Rotational stiffness	k_r	Top	750	639	Nm/rad
		1	236	185	Nm/rad
		2	103	79	Nm/rad
		3	—	38	Nm/rad
Normal stiffness	k_n	Top	5.92E7	5.81E7	N/m
		1	6.92E7	6.64E7	N/m
		2	8.00E7	7.43E7	N/m
		3	—	8.28E7	N/m
Shear stiffness	k_s	Top	1.69E6	3.69E6	N/m
		1	0.73E6	0.68E6	N/m
		2	0	0.27E6	N/m
		3	—	0	N/m

comparison shows no difference between the analytical and FEM model in terms of kinematic performance, thus validating the presented model. The results of the required joint slipper rotational stiffness with respect to the rotational joint directly connected to the slipper can be seen in Figure 12(b). If the ratio between the rotational stiffness of the slipper and that of the first joint connecting to the slipper is high, this means the angular rotation the slipper makes can be neglected in the total performance of the system.

The validated kinematic model can thus be used to determine the difference between the three different embodiments (Figure 13). Again, only the leftmost joint angle of each layer is shown since the remaining joints in the same layer show equal behavior with the difference of a phase shift.

The obtained kinematics are used to find the rotational stiffness, maximum normal force, and maximum shear force acting on each individual joint. The resulting determination of stiffness cases for the embodiments can be seen in Table 3.

Discussion

The results concerning the use of the design model and results from the case study will be both discussed.

Case study

A case study has been presented to show how the design model can be implemented, and what kind of performance can be expected by adding a whiffletree as bearing support. The model consists of defining the dimensions, kinematics, and kinetostatics given a

certain whiffletree layer set. Given a pre-defined total bearing length of $L_{tot} = 0.5\lambda$, with λ being the cam ring wavelength, it can be seen in Figure 11 and Table 2 that the whiffletree positively influences the Bearing Kinematics. This can be seen in the fact that the total height decreases of the bearing when increased whiffletree layers are implemented. It however also shows that in the given design case, the increase from a double to triple layer whiffletree only marginally improves the footprint and kinematic performance. Figure 13 shows the joint pivot angles for the FEM and analytical model. The results obtained from the FEM and analytical models have no noticeable difference, thus validating the design model presented in Sec.

From the results presented in Figure 13 it can be seen that the whiffletree behaves differently when moving through the concave and convex configurations of the track. Looking at the joint pivot angles shown in Figure 13, it is shown that the addition of whiffletree layers has a negligible small impact on the change in magnitude of the joint pivot angles for the different layers. This means that the top joint in a single layer whiffletree more or less rotates in a similar order of magnitude compared to a whiffletree support with several layers. This can be explained by looking at the angle of the corresponding linkage with the horizontal. The angle of the linkage is approximately equal to the angle of the gradient of the track at equal position. An increase in whiffletree layers does not change this orientation. Thus, no significant change in joint pivot angle is noted due to an increase in whiffletree angles. The top joint thus retains the largest rotational angle and will always be a limiting component in a deformable bearing design. The ratio between the rotational and normal stiffness[17] gives some indication on the severity of the design challenge. These have subsequently been calculated for the different embodiments, seen in Table 4. The results described here show that the

Table 4. Dimensional normal to rotational stiffness that gives an indication of the required performance for the contact-free joint implementation.

Layer	Double layer bearing	Triple layer bearing
Top (rad/m^2)	7.89E4	9.09E4
First (rad/m^2)	29.32E4	35.82E4
Second (rad/m^2)	77.67E4	94.05E4
Third (rad/m^2)	—	217.89E4

increased number of layers in the whiffletree positively influences the top stiffness ratio, which comes at the cost of a higher required performance at the third layer. Depending on the type of joints used, this stiffness requirement may prove to be critical. The required stiffness ratio described in this example would be at the limits of compliant joints as seen in literature,[17] and may require the development of alternatives. On the other hand, the minimum required shear stiffness is lower then the minimum required normal stiffness.

Finally, it is shown that an increase in whiffletree layers results in a decrease in slipper length, and thus a decrease in required compression of each slipper. The slipper pivot angle is shown in Figure 12 for a rotational stiffness ratio between slipper and bottom layer joint for one, two, and three orders of magnitude. It is shown that for a ratio of three orders of magnitude, no noticeable change in slipper pivot angle is noted. Meaning that a rotational stiffness ratio between slipper and bottom layer joint of at least three orders of magnitude is desired.

Model limitations

The design model provides a method to design a 2D whiffletree supported large deforming hydrostatic bearing. There are a few limitations to this design. Firstly, conventional hinge joints are used in the model compared to the preferred compliant joints. This is done for modeling purposes and the friction that occurs in conventional contact joints is neglected in this study. This is done since rigid body mechanics can be used in combination with the conventional hinge joints. Furthermore, it is assumed that the center of rotation stays at the same place while using compliant joints in the system. Since the scope of this project is to find a general solution regarding the kinematics and kinetostatics, and this simplification is valid. Secondly, the total perimeter of the bearing increases when multiple smaller slippers are connected together compared to a single slipper of equal length and width. The increase in bearing perimeter results in an increase in fluid losses of the bearing. The perimeter of the bearing, and thus the fluid losses, can be reduced by connecting all

slippers together thereby creating a single slipper that consists of multiple segments connected by elastic joints. This will also change the pressure profile from the single slippers as shown in Figure 10 to a continues pressure profile which can be described by a higher order polynomial. It is recommended to look into the behavior of this single continuous slipper in future research. Thirdly, the total joint length is restricted by the total linkage length. This is shown in the assumption that the bottom layer joint has a length of half the slipper length and each ascending joint is twice the length of the joint one layer below, resulting in the maximum allowable bearing length on each linkage. Fourthly, this work gives an explanation for the static and quasi-static state of a whiffletree supported hydrostatic bearing. Further research can be conducted to find the possible changes in results when perturbations and stability parameters in the dynamic state are taken into account. Finally, the slippers are geometrically not limiting the model and thus placed directly next to each other. In reality, when the bearing moves into a concave configuration, the slippers need to pass through each other which results in jamming. This can be solved by either using less of the maximum bearing design space or adding a gap between the slippers large enough such that the slipper can pass without contact. The latter option needs to follow from an extension of the model, to determine this exact gap dimension without influencing the bearing dimensions to much.

Conclusions

This work shows the potential of a whiffletree support system to increase the capability of 2D compliant hydrostatic bearings to follow non-constant curvature counter surfaces. An approximately quadratic relation is found between the slipper compression and length, and thus the required slipper compression is reduced for a decrease in slipper length. It is shown that an increase in whiffletree layers does not greatly affect the joint pivot angles of the ascending layers. However, the addition of extra layers in the whiffletree does lower each individual slipper length, reducing the required compression of the slipper. A ratio of at least three orders of magnitude between the slipper tilt stiffness and bottom layer joint is required to show no noticeable influence caused by the tilting of the slipper. Finally, the whiffletree can be used to rotate smaller slippers reducing their required compression while maintaining load capacity.

Declaration of conflicting interests

ORCID iD

Joep Nijssen https://orcid.org/0000-0002-5858-4673

References

1. Nijssen JPA and van Ostayen RAJ. Compliant hydrostatic bearings utilizing functionally graded materials. *J Tribology* 2020; 142: 1–9.
2. van Beek A and Segal A. Rubber supported hydrostatic thrust bearings with rigid bearing surfaces. *Tribol Int* 1997; 30: 47–52.
3. van Ostayen RAJ, van Beek A and Ros M. A mathematical model of the hydrosupport: an elasto-hydrostatic thrust bearing with mixed lubrication. *Tribol Int* 2004; 37: 607–616.
4. van Beek A and Lepic L. Rubber supported hydrostatic thrust bearings with elastic bearing surfaces of infinite length. *Wear* 1996; 201: 45–50.
5. Liang X, Yan X, Ouyang W, et al. Thermo-elasto-hydrodynamic analysis and optimization of rubber-supported water-lubricated thrust bearings with polymer coated pads. *Tribol Int* 2019; 138: 365–379.
6. Hooke C. Elastohydrodynamic lubricated of soft solids. In: Dowson D, Taylor CM and Childs THC (eds.) *Elastohydrodynamics –'96 fundamentals and applications in lubrication and traction. Tribology Series, vol. 32*. Birmingham: Elsevier, 1997, pp.185–197.
7. Nijssen J, Kempenaar A and Diepeveen N. Development of an interface between a plunger and an eccentric running track for a low-speed seawater pump. In: *Proceedings of the 11th international fluid power conference*, Aachen, 19–21 March 2018, pp.370–379.
8. Belyi A, Osadchy G, Efano D, et al. Implementation of the continuous monitoring system for technical condition of the St. Petersburg arena stadium sliding roof. In: *Proceedings of 2018 IEEE east-west design and test symposium, EWDTS*, Kazan, Russia, 2018, pp.1–10.
9. Stachowiak GW and Batchelor AW. *Engineering tribology*. 4th ed. Boston, MA: Butterworth-Heimann, 2014.
10. Liu Z, Wang Y, Cai L, et al. A review of hydrostatic bearing system: researches and applications. *Adv Mech Eng* 2017; 9: 1–27.
11. Kim R, Balakirsky S, Ahlin K, et al. Enhancing payload capacity with dual-arm manipulation and adaptable mechanical intelligence. *J Mech Robot* 2021; 13: 1–10.
12. Tamai R and Spyromilio J. European Extremely Large Telescope: progress report. In: *Ground-based and Airborne Telescopes V*, Quebec, 2014; 510 –518.
13. Baffes C, Mast T, Nelson J, et al. Primary mirror segmentation studies for the Thirty Meter Telescope. *Adv Opt Mech Technol Telesc Instrum* 2008; 7018: 266–280.
14. Nijenhuis J, Hamelinck R, Braam B, et al. Meeting highest performance requirements for lowest price and mass for the M1 segment support of the E-ELT. In: *Ground based and airborne telescope*, San Diego, 2010, vol. 3, p.7733.
15. Kazama T. Mixed lubrication simulation of hydrostatic spherical bearings for hydraulic piston pumps and motors. *J Adv Mech Des Syst Manuf* 2008; 2: 71–82.
16. Tian Y, Shirinzadeh B, Zhang D, et al. Three flexure hinges for compliant mechanism designs based on dimensionless graph analysis. *Precis Eng* 2010; 34: 92–100.
17. Gomes R, van Ostayen RAJ and Nijssen JPA. Design of a compliant hinge based on closed form pressure balancing. In: *Proceedings of the ASME 2020 international design engineering technical conference and computers and information in engineering conference, Volume 10: 44th mechanisms and robotics conference (MR)*, Virtual, Online, 17–19 August 2020, pp.370–379.
18. Xie Y, Yu J and Zhao H. Deterministic design for a compliant parallel universal joint with constant rotational stiffness. *J Mech Rob* 2018; 10: 1–12.
19. Yastrebov VA, Anciaux G and Molinari JF. The contact of elastic regular wavy surfaces revisited. *Tribol Lett* 2014; 56: 171–183.
20. Gao YF, Bower AF, Kim KS, et al. The behavior of an elastic–perfectly plastic sinusoidal surface under contact loading. *Wear* 2006; 261: 145–154.
21. Zhang Y, Finger S and Behrens S. *Introduction to mechanisms*. Pittsburgh, PA: Carnegie Mellon University, 2010.
22. Mulders SP, Diepeveen NFB and van Wingerden JW. Control design, implementation, and evaluation for an in-field 500 kW wind turbine with a fixed-displacement hydraulic drivetrain. *Wind Energy Sci* 2018; 3: 615–638.